

## Continuous cooling precipitation diagram of cast aluminium alloy Al–7Si–0.3Mg

Benjamin MILKEREIT<sup>1,2</sup>, Hannes FRÖCK<sup>1</sup>, Christoph SCHICK<sup>2</sup>, Olaf KESSLER<sup>1</sup>

1. Chair of Materials Science, Faculty of Mechanical Engineering and Marine Technology, University of Rostock, Germany;
2. Polymer-Physics Group, Institute of Physics, University of Rostock, Germany

Received 17 October 2013; accepted 30 April 2014

**Abstract:** The precipitation behaviour during quenching of cast Al–7Si–0.3Mg aluminium alloy was investigated by DSC in the cooling rate range of 0.01 K/s to 3 K/s and by quenching dilatometry for higher rates. Two main precipitation reactions were observed during cooling, a high temperature reaction starting almost directly with quenching from 540 °C and a low temperature reaction starting at about 400 °C. Quenching with 3 K/s already significantly suppresses precipitation during quenching. Hardness after T6 ageing increases with increasing quenching rate, due to the increasing content of supersaturated solid solution. By dilatometry and hardness results the critical cooling rate can be estimated as about 60 K/s. Quenched Al–7Si–0.3Mg microstructures have been investigated by light microscopy. The microstructures consist of an aluminium–silicon eutectic structure, aluminium solid solution dendrites and precipitates inside the aluminium dendrites, depending on quenching rate.

**Key words:** cast aluminium alloy; Al–7Si–0.3Mg; quenching; continuous cooling; precipitation diagram; differential scanning calorimetry; critical cooling rate

### 1 Introduction

Age hardening is the most important heat treatment to increase the strength of aluminium alloys. This is also applied to cast aluminium alloys. The age hardening procedure consists of solution annealing, quenching and ageing. Wrought aluminium alloys are mostly heat treated in semi-manufactured form whereas in the case of cast aluminium alloys typically the whole component is heat treated. By casting, shapes near construction geometry can be formed. Hence, quenching is critical for cast products especially with respect to distortion. Quenching in water bath is an easy and often applied method. Caused by the Leidenfrost effect, water quenching typically leads to nonuniform cooling over the component geometry. This fact results in large temperature gradients which might lead to distortion and residual stresses. In order to design optimal quenching processes or in order to simulate resulting distortion and residual stresses by a given quenching process, the knowledge about the precipitation behaviour and

mechanical properties during cooling (at each time and temperature) is essential [1,2]. However, the data are typically not available. An optimal quenching process has two contrary requirements. To gain the maximum strength, quenching must be done as fast as needed; On the other hand, for the minimal distortion, quenching should be done as slow as possible. In order to optimize quenching, at least the critical quenching rate must be known. In detail the upper critical quenching rate is defined as the slowest cooling rate at which every diffusion controlled precipitation during quenching is suppressed and the whole amount of solved alloying element atoms remain in supersaturated solid solution [3]. Continuous cooling precipitation (CCP) diagrams show the precipitation behaviour of aluminium alloys during cooling from solution annealing as functions of temperature and time [3–7]. Those diagrams typically give information about quenching sensitivity of aluminium alloys. The quenching sensitivity of aluminium alloys has been frequently investigated over the past three decades [8–15]. In the most reports, quenching sensitivity was investigated experimentally

using different quenching media to obtain different cooling rate ranges [8,12,14,15]. Another important part of the experimental work was done by the Jominy end quenching method [9,13] and interrupted and delayed quenching [14]. However, quenching sensitivity of cast aluminium alloys is less well investigated than that of wrought aluminium alloys. Some authors modelled C-curves from classical [9] and improved methodology for quenching factor analysis [14]. Both works used Jominy end quenching results as experimental database. SJÖLANDER and SEIFEDDINE [16] in 2010 published a review about heat treatment of cast Al–Si–Cu–Mg alloys. With respect to quenching from solution annealing, they summarised the results for yield strength as function of quenching rate from several authors with a relative large cooling rate range of five orders of magnitude including four different types of cast Al–Si–Mg alloys. Basically, yield strength increases with increasing cooling rate. Some of the alloys seem to reach a saturation level at higher rates. The critical cooling rates are to expect in a cooling rate region of some K/s to some 100 K/s. Related to wrought Al–Mg–Si alloys with the same Mg content, the critical cooling rates are significantly higher for cast Al–Si–Mg alloys [7,16].

In the previous work, we developed a technique to record continuous cooling precipitation diagrams for wrought aluminium alloys over the entire range of cooling rates of technical and physical interest: from slow cooling close to equilibrium condition up to complete supersaturation (also for the high alloyed wrought 7049A alloy [17]) using a combination of different types of differential scanning calorimeters (DSC), quenching dilatometry and microstructure analysis [3,7,17–19]. Microstructures of wrought and cast aluminium alloys differ significantly. Wrought alloys mainly consist of aluminium solid solution, whereas cast alloys contain large amount of eutectic structures like aluminium–silicon. One main difference between age hardening of wrought and cast alloys is solution annealing duration. Wrought aluminium alloys have been homogenisation-annealed before age hardening and solution annealing typically takes only for some 10 min [20]. During solution annealing of cast alloys, homogenisation and dissolution of age hardening elements occur. Hence, solution annealing of cast aluminium alloys typically takes for some hours [20]. These differences between cast and wrought alloys influence the continuous cooling precipitation diagrams. The DSC method has several experimental advantages compared to the other methods: Cooling can be performed either with controlled linear cooling [3] or

with defined nonlinear cooling in the case of real air or gas cooling [18]. Additionally, the reaction start and end temperatures can be evaluated relatively easily. A special benefit to other methods is that by the DSC signal the precipitation heat or enthalpy [3] can be evaluated. The precipitation heat indicates the intensity of the reaction and is related to the amount of mass fraction precipitated [7]. Generally, the DSC method seems to be an effective and meaningful experimental method to investigate quenching sensitivity of aluminium alloys. Therefore, the purpose of this work is to gain a first step to experimentally record continuous cooling precipitation diagram for an Al–7Si–0.3Mg (A356) over a wide range of cooling rates and to show that the DSC method is also suitable for aluminium cast alloys.

## 2 Experimental

In this work cast Al–7Si–0.3Mg (EN AC-42100/A356) aluminium alloy was investigated. Figure 1 shows foundry components produced by mould casting. Samples were machined from automobile sockets bearing the suspension struts [21]. The chemical composition of the cast batch is given in Table 1. Figure 2 shows the initial “as-cast” microstructure gained by an optical microscope with differential interference contrast (DIC). Next to the aluminium solid solution an eutectic microstructure is visible.

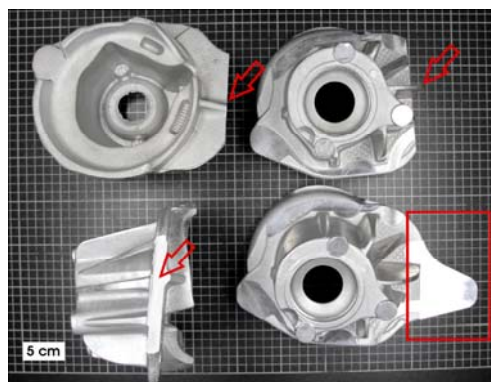


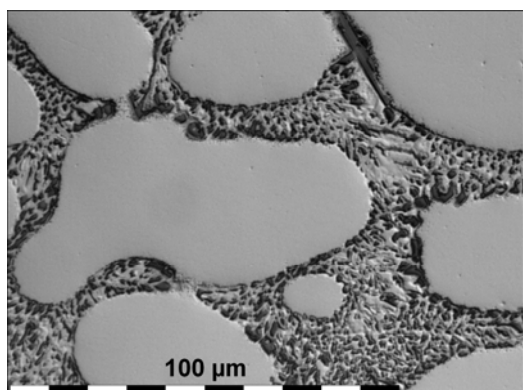
**Fig. 1** Foundry components in different views (Automobile sockets bearing suspension struts, produced by mould casting [21]. Rectangle and arrows indicate location of obtained DSC samples)

High quality DSC measurements of precipitation reactions in aluminium alloys require an inert reference material which has about the same absolute heat capacity to measure excess specific heat [3]. For this work pure aluminium with a purity of 99.9995% was used as reference.

In order to investigate a large range of cooling rates, three types of differential scanning calorimeters (DSC)

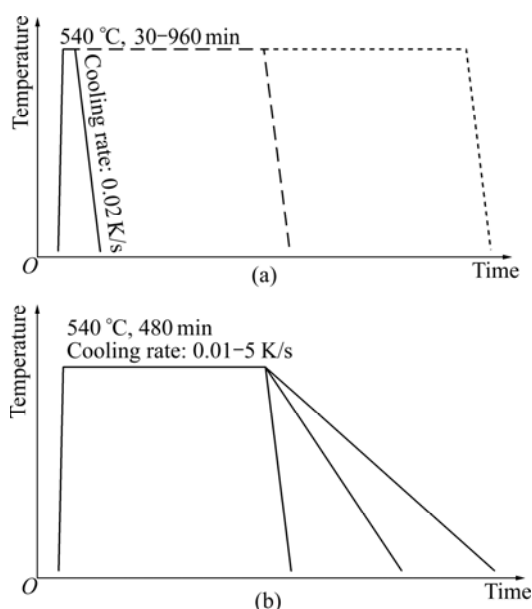
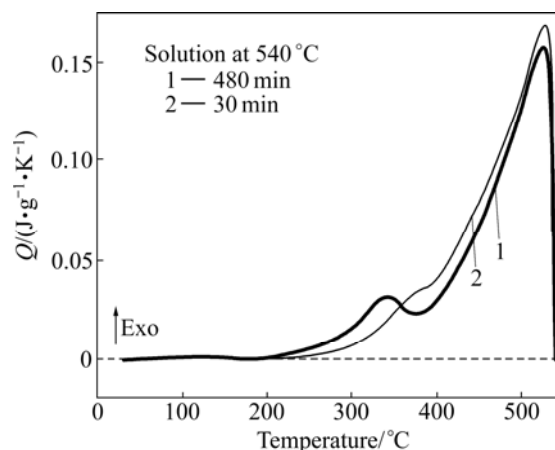
**Table 1** Chemical composition of investigated batch of Al–7Si–0.3Mg (mass fraction,%)

Alloy	Si	Fe	Cu	Mn	Mg	Ti	Al
Al–7Si–0.3Mg	7.31	0.092	0.005	0.005	0.31	0.13	Residue
EN AC-42100	6.5–7.5	<0.19	<0.05	<0.10	0.25–0.45	0.08–0.25	Residue

**Fig. 2** Optical microscope DIC showing as-cast microstructure after etching with Weck's reagent [22]

were used. The slowest device is a Calvet-type [23] Setaram 121 DSC which covers a cooling rate range from about 0.01 K/s to 0.1 K/s. Cylindrical samples with a diameter of 5.7 mm and a length of 21.7 mm were investigated. The sample mass was about 1468 mg. Samples were packed in standard 300  $\mu$ L aluminium crucibles. The cooling rate range from 0.2 to 0.5 K/s was analyzed with a Mettler Toledo 823 DSC. For this device flat cylindrical samples with a diameter of 5.4 mm and a length of 1.4 mm were optimal. The samples had a mass of about 82.5 mg and were packed in aluminium crucibles with pin. The lid of the crucibles was laid on top loosely. The fastest used DSC was a Perkin Elmer Pyris 1 DSC covering the cooling rate range of 0.5–5 K/s. For this device, flat cylindrical samples with a diameter of 6.4 mm and a length of 1.0 mm were used. The sample mass was adjusted to about 83.5 mg and the samples were packed in standard aluminium crucibles. Details of the measurement procedure can be seen in Ref. [3]. Evaluation of the data was done as described in Ref. [18]. The solution annealing duration was analyzed in preliminary investigations. To conclude the needed annealing duration, the precipitation behaviour during relatively slow cooling with 0.02 K/s was analyzed after solution annealing with varying durations between 30 to 960 min (0.5–16 h). Schematically, the temperature–time profile is shown in Fig. 3(a). It was found that after 30 min, the precipitation heat (enthalpy) is about the same as all longer investigated solution annealing durations. Thereby, it can be concluded that the whole amount of alloying elements which can be solved at 540  $^{\circ}$ C is already in solid solution. Nevertheless, also differences

between the precipitation behaviour after different solution annealing durations were found as presented in Fig. 4. In Fig. 4 two DSC cooling curves with a relative slow cooling rate of 0.02 K/s are shown. The curves were obtained with a Setaram 121 DSC and calculated to be excess specific heat [3]. Next to the DSC curves the zero level is shown as dotted line. Deviations above this level indicate exothermal reactions. The used cooling

**Fig. 3** Schematic time–temperature profile: (a) Solution annealing; (b) Precipitation behaviour during cooling from solution annealing**Fig. 4** DSC cooling curves of Al–7Si–0.3Mg with cooling rate of 0.02 K/s after different solution annealing durations at 540  $^{\circ}$ C

rate of 0.02 K/s is within the optimal cooling rate range of this device.

Basically, both measurements show a similar behaviour, namely, two main exothermal precipitation reactions are visible: a high temperature reaction peak between about 540 °C to 400 °C followed by a low temperature reaction peak down to about 200 °C. Both reactions overlap each other. After short solution annealing of 30 min the high-temperature reaction is slightly stronger than after 480 min solution annealing. More obviously, after 480 min solution annealing the low-temperature reaction becomes more pronounced compared to 30 min solution annealing. From the previous work it is known for wrought Al–Mg–Si alloys that the high temperature reactions belong to precipitation of equilibrium phase  $\beta$ -Mg<sub>2</sub>Si parallel with precipitation of excess Si [7]. Nucleation of Mg<sub>2</sub>Si happens mostly heterogeneously at primary precipitates distributed relatively coarse. Beside, the low-temperature reactions belong to precipitation of precursor phases like  $\beta'$  and  $B'$ . The distribution of these phases is much finer compared to the high temperature phases [7]. Having this knowledge in mind we conclude that after 30 min at 540 °C the whole possible amount of alloying elements is already solved, but it is much more evenly distributed after annealing for at least 480 min (8 h). Longer solution annealing does not show any changes in the precipitation behaviour. Hence, to ensure a highest possible homogeneity but also shortest possible one, 480 min was determined as solution annealing duration.

For the main investigation, precipitation behaviour during cooling from solution annealing at 540 °C for 480 min was analyzed (Fig. 3(b)). Several experiments with 15 different cooling rates were performed covering about three orders of magnitude. Each cooling rate was measured at least two times. Additionally, at least one baseline experiment was measured in-between the two sample measurements. This is a relative small amount compared to the previous work [3]; however, the long solution annealing duration limited the amount of experiments. To gain information about the influence of cooling on the final mechanical properties Vickers hardness was tested ( $HV_1$ ). Therefore, samples were aged artificially directly after cooling. The storage duration at room temperature in-between was kept at about 5 min. Artificial ageing was performed at 160 °C for 360 min. For cooling rates faster than 3 K/s, a quenching dilatometer Baehr 805 AD was used.

Additionally, the microstructure was analyzed with an optical microscope. Samples for light microscopy were prepared by standard grinding and polishing with water-free, ethanol-based lubricants. To identify the location of precipitates, the specimens were etched for a

few seconds in Weck's reagent (a solution of 4 g potassium permanganate in 100 mL distilled H<sub>2</sub>O and 1 g sodium hydroxide [22]). After etching, an etch-skin remained on the surface, which was removed by cautious polishing.

### 3 Results and discussion

Figure 5 shows seven characteristic DSC cooling curves as a function of temperature for cast Al–7Si–0.3Mg aluminium alloy. The curves are arranged in order of increasing cooling rate, starting with the slowest rate on top. The dotted line in each DSC curve represents the zero level. Deviations above this level indicate exothermal reactions.

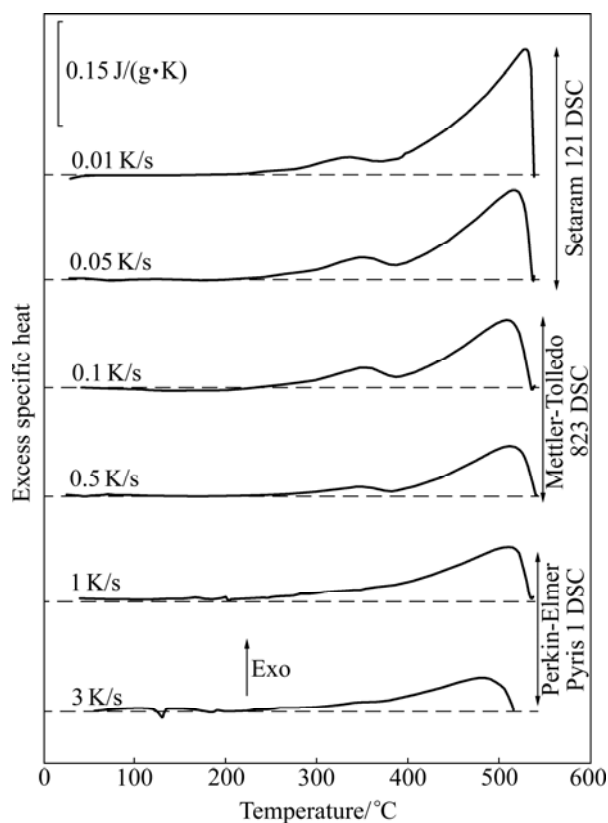


**Fig. 5** Selected DSC cooling curves of investigated composition of cast Al–7Si–0.3Mg alloy after solution annealing at 540 °C for 480 min (Curves were obtained from three different types of DSC devices corresponding to different cooling rates from 0.01 to 3 K/s)

On the first view, the basic precipitation behaviour shows high similarities compared to wrought Al–Mg–Si alloys, namely, two main reaction peaks are detectable, a high temperature and a low temperature peaks [3,7]. It may be expected that several precipitation reactions belong to each main reaction peak, respectively, as also known from wrought Al–Mg–Si alloys [7].

At slow cooling, the high-temperature reactions

(HTR) started directly with onset of cooling. At faster cooling rates, this cannot be observed with certainty, because of the time that the device needs to settle steady state cooling. This results in a heat flow peak which is cut here. The high-temperature reactions get increasingly suppressed with increasing cooling rate. The direct start of precipitation was expected at least for slow cooling, because the amount of alloying elements is above solubility at 540 °C.

Following the high-temperature reactions, low-temperature reactions (LTR) occur in a temperature range of about 370 to 250 °C. As it is hardly visible by eye (but is more obvious from Fig. 5), the intensity of the low-temperature reactions first slightly increase up to about 0.1 K/s, but finally also the low-temperature reactions get suppressed with increasing rates above 0.1 K/s. This behaviour is also known from wrought Al–Mg–Si alloys [3,7,18,19,24] and can be explained by the higher amount of remaining solved alloying elements available for the low-temperature reactions because the high-temperature reactions are already significantly suppressed.

Nevertheless, opposite to wrought Al–Mg–Si alloys, the high-temperature reactions are always dominant, the precipitation heat of the high-temperature reactions is higher in the whole investigated cooling rate range. For wrought Al–Mg–Si alloys, it was found previously that at the cooling rate the high-temperature reactions are already strongly suppressed, the low-temperature reactions become more dominant and release a large amount of precipitation heat [3,7,18,19,24].

This difference might be explained by the much higher amount of excess Si. As it is known for wrought Al–Mg–Si alloys next to the precipitation of Mg<sub>2</sub>Si,

precipitation of excess Si belongs to the high-temperature reactions. Hence, it seems to be reasonable that precipitation of excess Si dominates the high-temperature reactions in the cast alloy.

Another observation which is opposite to wrought Al–Mg–Si alloy is that the peak shifts observed for cast Al–7Si–0.3Mg alloy are rather small in the investigated cooling rate range.

The precipitation start and end temperatures were taken from DSC curves as shown in Fig. 5 and plotted in a temperature–time diagram. The resulting CCP diagram of Al–7Si–0.3Mg is shown in Fig. 6. The detected precipitation start and end temperatures are indicated by different symbols. The CCP diagram provides information regarding precipitation reactions as a function of the cooling rate and temperature. Another important piece of information is the intensity of the precipitation reactions.

This intensity can be evaluated from the peak areas of the DSC curves in Fig. 5 and is displayed in Fig. 7 for the investigated cast Al–7Si–0.3Mg alloy. The specific precipitation heat during cooling to room temperature as well as the hardness after ageing as a function of the cooling rate are presented. The cooling rate axis follows an increasing logarithmic scale for comparison with the time scale of the CCP diagrams. Thus, Figs. 6 and 7 are complementary. For the precipitation heat, the error bars show the minimal and maximal measured precipitation heat. For the hardness values, the standard deviation calculated from six indentations is shown.

Overall precipitation heat decreases continuously with increasing cooling rate from about 16 J/g down to about 6.5 J/g. The same trend was detected for the precipitation heat of the high-temperature reactions,

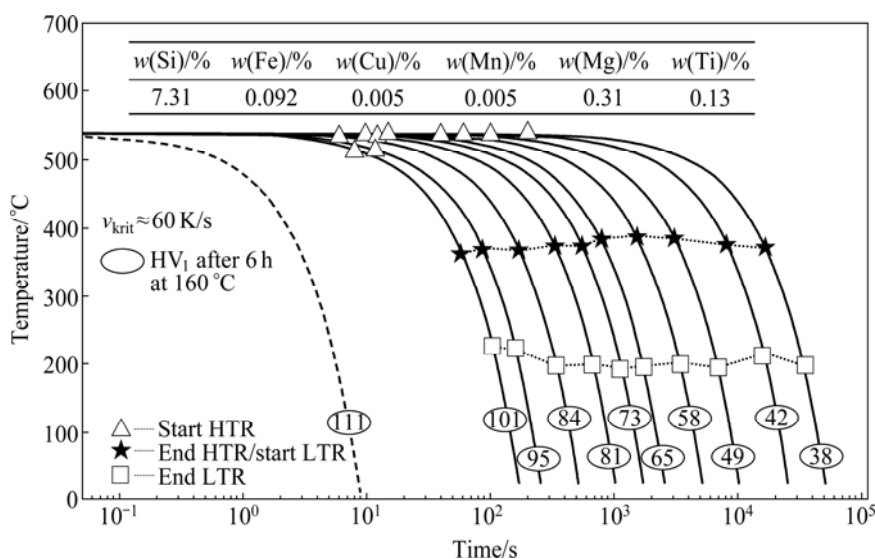


**Fig. 6** Continuous cooling precipitation diagram of investigated composition of Al–7Si–0.3Mg after solution annealing at 540 °C for 480 min

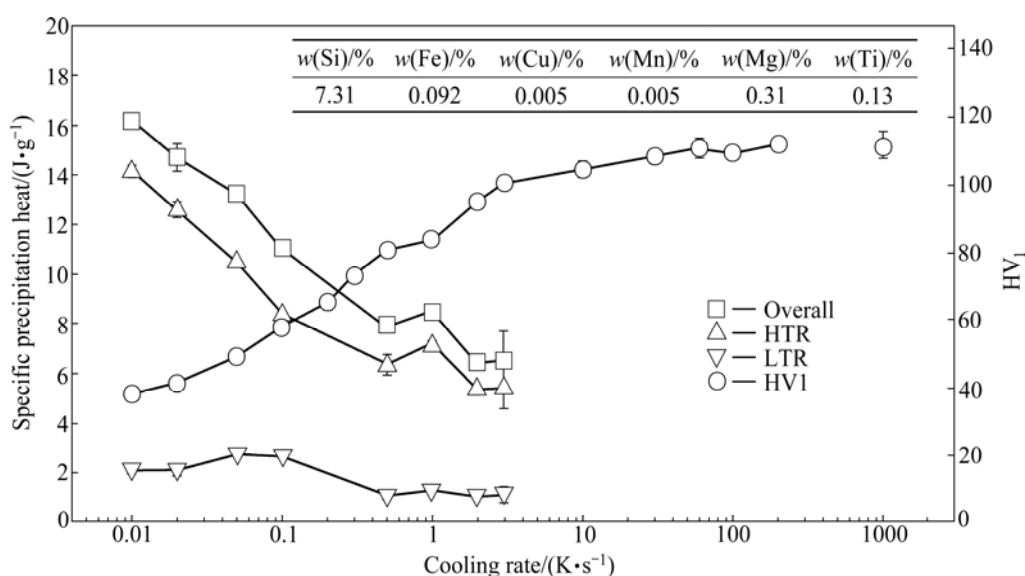


**Fig. 7** Specific precipitation heats for high-temperature reaction (HTR), low-temperature reaction (LTR) and sum of all (overall) reactions after cooling to room temperature from solution annealing at 540 °C for 480 min as well as Vickers hardness after additional artificial ageing at 160 °C for 360 min for investigated composition of Al-7Si-0.3Mg as functions of cooling rate

which decreases from about 14 J/g at 0.01 K/s down to about 5 J/g at 3 K/s. Whereas the intensity of the low-temperature reactions changes only slightly. Starting from about 2 J/g at the slowest investigated cooling rate, the precipitation heat slightly increases to about 3 J/g in a range between 0.05 K/s to 0.1 K/s. At rates faster than 0.1 K/s the precipitation heat decreases down to about 1 J/g at the fastest rate measured with DSC, 3 K/s.

The hardness after aging continuously increases with increasing cooling rate from about HV<sub>1</sub> 40 at 0.01 K/s to a maximum of about HV<sub>1</sub> 112 at 200 K/s. Already at 60 K/s with about HV<sub>1</sub> 111, the hardness reaches its maximum level. Next to the heat treatment with the DSC devices and the dilatometer, some samples were quenched in water at about 20 °C. Due to the small samples with a diameter of about 6 mm and a length of about 22 mm, it is to expect that cooling is rather fast. Probably about 1000 K/s was reached at least in the temperature range between 400 °C and 290 °C estimated according to OSTERMANN [25] (Figure 3.2.43 on page 179). The obtained hardness value of HV<sub>1</sub> 111 fits perfectly the maximum hardness level tested for this alloy. Therefore, it can be concluded that the critical cooling rate of this alloy is about 60 K/s.

In comparison to wrought Al-Mg-Si alloys with about the same Mg content this critical cooling rate is rather fast. For example, for 6060 with the mass fractions of 0.4% Si, 0.44% Mg, an upper critical cooling rate of 0.83 K/s, for 6005A with the mass fractions of 0.68% Si, 0.57% Mg, an upper critical cooling rate of 6.25 K/s and for 6082 with the mass fractions of 0.69% Si, 0.62% Mg, an upper critical cooling rate of 16.67 K/s, were

determined earlier [3,7]. The cast alloy investigated here has only a mass fraction of 0.31% Mg. This indicates that for cast Al-Si-Mg alloys the Si content is a driving force for the quenching sensitivity. From wrought alloys it is known that precipitation of silicon belongs to the high-temperature reactions, therefore it can be assumed that this can be applied to Al-Si-Mg cast alloys too. The high amount of excess Si then can explain the dominance of the high-temperature reactions but also the high critical cooling rates.

Figure 8 shows five optical microscopy images after different cooling rates between 0.01 K/s and 200 K/s. After solution annealing and cooling in all images next to aluminium solid solution the eutectic structure is visible. Compared to the as-cast structure, the silicon particles are coarsened by solution annealing.

By etching, the secondary precipitates inside the aluminium solid solution are made visible. At slow cooling few precipitates are inside the centre of the aluminium solid solution dendrites. Precipitation-free zones around the centres of the dendrites are found towards eutectic region. The high amount of precipitates are formed during slow cooling, but rather at the eutectic silicon, than in the aluminium dendrites. With increasing cooling rate, silicon diffusion out of the aluminium dendrites is suppressed and precipitates form inside the dendrites. Further increasing cooling rate also suppresses precipitation inside the aluminium dendrites.

At 0.3 K/s inside aluminium solid solution, some needle-shaped precipitates are best observed. It is remarkable that inside of one dendrite, those needle-shaped precipitates are aligned parallel or perpendicular

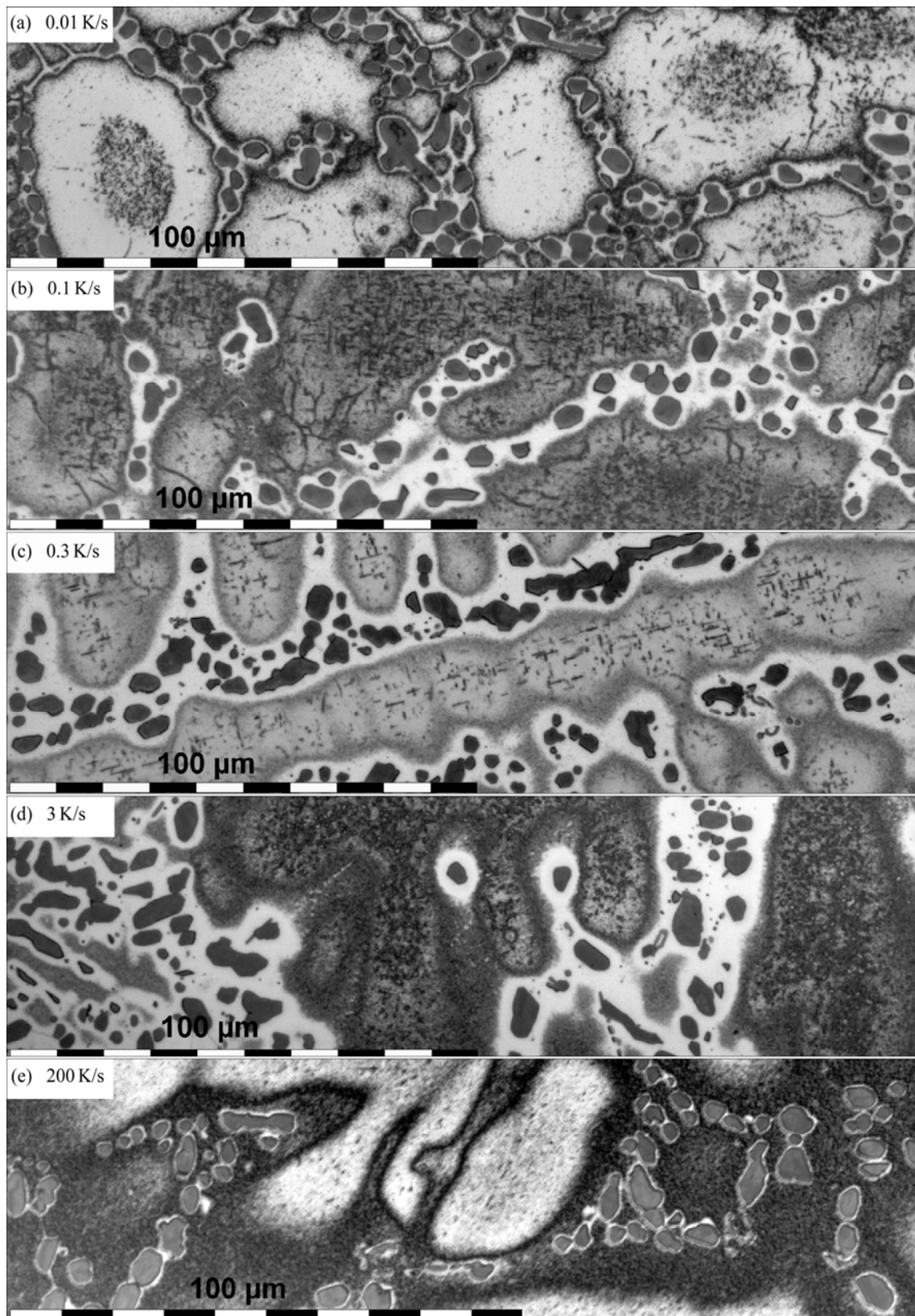


**Fig. 8** Optical microscopy images of Al-7Si-0.3Mg samples after cooling with different rates and etching with Weck's reagent [22]

to each other. Those precipitates grow along distinct lattice planes, such as  $\langle 100 \rangle$  planes of the aluminium solid solution.

At 3 K/s, no precipitation-free zones are found inside the aluminium solid solution dendrites. Moreover, the dendrites are full with precipitates. Those precipitates

are much finer distributed inside the aluminium solid solution dendrites compared to at 0.3 K/s. At the fastest investigated cooling rate of 200 K/s, the aluminium solid solution seems to be free from quenching precipitates on the light microscopy level.

However, further intensive microstructure investigations with SEM and TEM need to be performed in the future.

## 4 Conclusions

1) The continuous cooling precipitation diagram of a batch of cast Al–7Si–0.3Mg was recorded by differential scanning calorimetry (DSC). Utilizing three different types of DSC devices and next to a quenching dilatometer, overall a cooling rate range of about four orders of magnitude was covered by linear cooling experiments (0.01–200 K/s).

2) DSC curves showed two main reaction peaks comparable to wrought Al–Mg–Si alloys. A difference from wrought alloys is that the high-temperature reactions dominate over the whole investigated cooling rate range. From wrought alloys it is known that precipitation of silicon belongs to the high-temperature reactions, therefore it can be assumed that this can be applied to cast Al–Si–Mg alloys too. The high amount of excess Si then can explain the dominance of the high-temperature reactions.

3) Microstructure investigations by optical microscope have been performed. At slow cooling rate, precipitation seems to concentrate in eutectic regions. At medium cooling rates inside the aluminium dendrites dark precipitates, which seem to be aligned to the distinct planes of the aluminium, are visible. At the highest investigated cooling rate of 200 K/s, no precipitates are visible inside aluminium dendrites.

4) The hardness was tested after different cooling rates and a final artificial ageing. By the hardness results it can be concluded that the critical cooling rate of this batch of cast Al–7Si–0.3Mg is about 60 K/s.

## References

- [1] REICH M, KESSLER O. Mechanical properties of undercooled aluminium alloys and their implementation in quenching simulation [J]. *Materials Science and Technology*, 2012, 28: 769–772.
- [2] REICH M, SCHÖNE S, KEBLER O, NOWAK M, GRYDIN O, NÜRNBERGER F, SCHAPER M. Simulation of gas and spray quenching during extrusion of aluminium alloys [J]. *Key Engineering Materials*, 2010, 424: 57–64.
- [3] MILKEREIT B, KESSLER O, SCHICK C. Recording of continuous cooling precipitation diagrams of aluminium alloys [J]. *Thermochimica Acta*, 2009, 492: 73–78.
- [4] HERDING T, KESSLER O, HOFFMANN F, MAYR P. An approach for continuous cooling transformation (CCT) diagrams of aluminium alloys [C]//GREGSON P J, HS J. 8th International Conference on Aluminium Alloys. Cambridge, UK: Trans Tech Publications Ltd, 2002: 869–874.
- [5] KESSLER O, von BARGEN R, HOFFMANN F, ZOCH H W. Continuous cooling transformation (CCT) diagram of aluminum alloy Al–4.5Zn–1Mg [C]//POOLE W J, WELLS M A, LLOYD D J. Proceedings of the 10th International Conference on Aluminium Alloys. Vancouver, 2006: 1467–1472.
- [6] LI Hong-ying, ZHAO Yan-kuo, TANG Yi, WANG Xiao-feng, DENG Yun-zhe. Continuous cooling transformation curve for 2A14 aluminum alloy and its application [J]. *The Chinese Journal of Nonferrous Metals*, 2011, 21(5): 968–974. (in Chinese)
- [7] MILKEREIT B, WANDERKA N, SCHICK C, KESSLER O. Continuous cooling precipitation diagrams of Al–Mg–Si alloys [J]. *Materials Science and Engineering A*, 2012, 550: 87–96.
- [8] CROUCHER T, BUTLER D. Polymer quenching of aluminum castings [C]//National SAMPE Symposium and Exhibition. Los Angeles: SAMPE, 1981: 527–535.
- [9] MA S, MANIRUZZAMAN M D, MACKENZIE D S, SISSON R D Jr. A methodology to predict the effects of quench rates on mechanical properties of cast aluminum alloys [J]. *Metallurgical and Materials Transactions B*, 2007, 38: 583–589.
- [10] NEWKIRK J W, LIU Q, MOHAMMADI A. Optimizing the aging heat treatment of cast aluminum alloys [C]//DAS S K, SKILLINGBERG M H. *Alumznum 2002: Proceedings of TMS 2002 Annual Meeting: Automotive Alloys and Aluminum Sheet and Plate Rolling and Finishing Technology Symposia*. Seattle, WA, 2002: 75–82.
- [11] PEDERSEN L, ARNBERG L. The effect of solution heat treatment and quenching rates on mechanical properties and microstructures in AlSiMg foundry alloys [J]. *Metallurgical and Materials Transactions A*, 2001, 32: 525–532.
- [12] CHAUDHURY S K, APELIAN D. Effects of fluidised bed quenching on heat treating characteristics of cast Al–Si–Mg and Al–Si–Mg–Cu alloys [J]. *International Journal of Cast Metals Research*, 2006, 19: 361–369.
- [13] NEWKIRK J W, MEHTA S. Studying the quench sensitivity of cast Al alloys [C]//FUNATANI K, TOTTE G E. *ASM Proceedings: Heat Treating Proceedings of the 20th Conference*. St. Louis, MO, 2000: 1094–1100.
- [14] TIRYAKIOĞLU M, SHUEY R T. Quench sensitivity of an Al–7 pct Si–0.6 pct Mg alloy: Characterization and modeling [J]. *Metallurgical and Materials Transactions B*, 2007, 38: 575–582.
- [15] ZHANG D L, ZHENG L. The quench sensitivity of cast Al–7 wt%Si–0.4 wt% Mg alloy [J]. *Metallurgical and Materials Transactions A*, 1996, 27: 3983–3991.
- [16] SJÖLANDER E, SEIFEDDINE S. The heat treatment of Al–Si–Cu–Mg casting alloys [J]. *Journal of Materials Processing Technology*, 2010, 210: 1249–1259.
- [17] ZOHRABYAN D, MILKEREIT B, KESSLER O, SCHICK C. Precipitation enthalpy during cooling of aluminum alloys obtained from calorimetric reheating experiments [J]. *Thermochimica Acta*, 2012, 529: 51–58.
- [18] MILKEREIT B, BECK M, REICH M, KESSLER O, SCHICK C. Precipitation kinetics of an aluminium alloy during Newtonian cooling simulated in a differential scanning calorimeter [J]. *Thermochimica Acta*, 2011, 522: 86–96.
- [19] MILKEREIT B, JONAS L, SCHICK C, KESSLER O. Das kontinuierliche Zeit-Temperatur-Ausscheidungs-Diagramm einer Aluminiumlegierung EN AW-6005A [J]. *HTM Journal of Heat Treatment and Materials*, 2010, 65: 159–171.
- MILKEREIT B, JONAS L, SCHICK C, KESSLER O. The continuous cooling precipitation diagram of an aluminum alloy EN AW-6005A [J]. *HTM Journal of Heat Treatment and Materials*, 2010, 65: 159–171.

- [20] POLMEAR I J. Light alloys [M]. Oxford: Butterworth-Heinemann, 2006.
- [21] ROSE A, KESSLER O, HOFFMANN F, ZOCH H W. Quenching distortion of aluminium castings—improvement by gas cooling [J]. Materialwissenschaft und Werkstofftechnik, 2006, 37: 116–121.
- [22] WECK E, LEISTNER E. Metallographische Anleitung zum Farbätzen nach dem Tauchverfahren Teil III: Nichteisenmetalle, Hartmetalle und Eisenwerkstoffe, Nickel-Basis- und Kobalt-Basis-Legierungen [M]. Düsseldorf: Deutscher Verlag für Schweißtechnik (DSV) GmbH, 1986.
- WECK E, LEISTNER E. Metallographic instruction for color etching by dipping principle. Part III: Nonferrous Metals, hard-metals and ferrus material, nickel-basic and cobalt-basic-alloys [M]. Düsseldorf: Deutscher Verlag für Schweißtechnik (DSV) GmbH, 1986.
- [23] CALVET E, PRAT H, SKINNER H. Recent progress in microcalorimetry [M]. Oxford, London, New York, Paris: Pergamon Press, 1963.
- [24] MILKEREIT B, OSTEN J, SCHICK C, KESSLER O. Continuous heating dissolution diagrams of aluminium alloys [C]/WEILAND H, ROLLETT A D, CASSADA W A. 13th International Conference on Aluminum Alloys (ICAA13). Pittsburgh, PA, USA: TMS (The Minerals, Metals & Materials Society), 2012: 1095–1100.
- [25] OSTERMANN F. Anwendungstechnologie aluminium [M]. Berlin: Springer, 2007.

## 铸态 Al-7Si-0.3Mg 合金的连续冷却析出图

Benjamin MILKEREIT<sup>1,2</sup>, Hannes FRÖCK<sup>1</sup>, Christoph SCHICK<sup>2</sup>, Olaf KESSLER<sup>1</sup>

1. Chair of Materials Science, Faculty of Mechanical Engineering and Marine Technology,  
University of Rostock, Germany;

2. Polymer-Physics Group, Institute of Physics, University of Rostock, Germany

**摘要:** 采用冷却速率为 0.01~3 K/s 的差示扫描量热法(DSC)和冷却速率更高的淬火膨胀法研究铸态 Al-7Si-0.3Mg 合金淬火的析出行为。在合金冷却的过程中发生了两种析出反应, 高温反应开始于淬火起始温度 540 °C, 低温反应始于 400 °C 左右。3 K/s 的淬火冷却速率已经显著抑制淬火过程中相的析出。合金 T6 态的硬度随着淬火速率的增快而增加, 这是由合金过饱和固溶度增加而导致的。通过膨胀实验和硬度实验的结果可以估计临界冷却速率大约为 60 K/s。通过光学显微镜观察淬火态的铸态 Al-7Si-0.3Mg 合金的显微组织。结果表明: 根据淬火冷却速率的不同合金的显微组织由铝-硅共晶组织、铝固溶体枝晶及枝晶间的析出相组成。

**关键词:** 铸态铝合金; Al-7Si-0.3Mg; 淬火; 连续冷却; 析出相图; DSC; 临界冷却速率

(Edited by Hua YANG)